Superfluidity and solid order in a two-component Bose gas with dipolar interactions in an optical lattice

Yoshihito Kuno, Keita Suzuki, and Ikuo Ichinose*
Department of Applied Physics, Nagoya Institute of Technology, Gokiso, Showa-ku, Nagoya 466-8555, Japan
(Received 10 October 2014; published 11 December 2014)

In this paper, we study an extended bosonic *t-J* model in an optical lattice, which describes two-component hard-core bosons with nearest-neighbor pseudospin interactions and, also, inter- and intraspecies dipole-dipole interactions. In particular, we focus on the case in which two-component hard-core bosons have antiparallel polarized dipoles with each other. The global phase diagram is studied by means of the Gutzwiller variational method and also quantum Monte Carlo (QMC) simulations. Both calculations show that a striped solid order, besides a checkerboard one, appears as a result of the dipole-dipole interactions. By QMC, we find that two kinds of supersolids (SSs) form, i.e., checkerboard SS and striped SS, and we also verify the existence of an exotic phase between the striped solid and the checkerboard SS. Finally, by QMC, we study the *t-J*-like model, which was recently realized experimentally by A. de Paz *et al.* [Phys. Rev. Lett. **111**, 185305 (2013)].

DOI: 10.1103/PhysRevA.90.063620 PACS number(s): 67.85.Hj, 67.80.kb, 67.85.Fg

I. INTRODUCTION

In recent years, cold-atomic systems have played a very important role in the study of condensed matter physics. In particular, the cold-atomic system in an optical lattice (OL) [1] is sometimes regarded as a feasible simulator to search for new types of quantum states. Cold-atomic systems in an OL are versatile and the effects of defect and impurity are negligibly small. With the use of quantum simulators, some important subjects have been studied, including strongly correlated systems [2], lattice gauge theory [3], and cosmology [4].

From the above point of view, we are interested in the exotic quantum state in cold-atomic gases called a supersolid (SS) [5], which has both a crystalline and a superfluid (SF) order. While many interesting works on this subject [6,7] have been reported for single-component cold atomic gases, the study on two-component boson systems is still inadequate. In the present paper, we study the bosonic *t-J* (B-t-J) model [8–11] with dipole-dipole interactions (DDIs) [12], as the long-range nature of the DDIs possibly generates interesting phases including the SS.

To study the phase diagram in detail, we employ both the Gutzwiller variational method and numerical quantum Monte Carlo (QMC) simulations. To perform the QMC, we use the effective field-theory model of the B-t-J model derived in the previous paper [13]. All relevant quantum fluctuations are included in the QMC stimulations of the effective model. The phase diagrams obtained by the above two methods are compared with each other and effects of the quantum fluctuations are discussed.

This paper is organized as follows. In Sec. II A, we introduce the B-t-J model and briefly explain the derivation of the effective-field theory. In the derivation, the hard-core constraint of the B-t-J model is faithfully treated by using the slave-particle representation. In Sec. II B, we consider the DDI and introduce its effects into the B-t-J model. In the present paper, we consider the case in which dipoles of two-component bosons are antiparallel to each other. In this case, the DDIs are nothing but z-component pseudospin interactions. Thus we call the resultant mode the extended B-t-J model. In Sec. III, we study the phase diagram using the Gutzwiller method, which is a kind of mean-field approximation. In Sec. IV, the results obtained by means of QMC are shown and discussed. A detailed investigation of the global phase diagram is given, in particular, states in the region of the competing orders of the solid and SF are discussed in detail. In Sec. V, we introduce and study an anisotropic B-t-J model (called the B-t-J-like model), which was recently realized experimentally [2]. By QMC, we show that the experimental observation is reproduced in the model. Section VI is devoted to the conclusion.

II. BOSONIC *t-J* MODEL WITH DDIS AND DERIVATION OF THE EFFECTIVE MODEL

A. Bosonic *t-J* model and the slave-particle representation

The system of a two-species Bose gas in an OL with strong on-site repulsions is often described by the B-t-J model. Its relationship to the Bose-Hubbard model has been discussed in previous papers. In the present paper, we regard the B-t-J model as a canonical model for a strong on-site repulsive Bose-gas system. The Hamiltonian of the B-t-J model is given as [8–11,14],

$$H_{tJ} = -\sum_{\langle i,j\rangle} t(a_i^\dagger a_j + b_i^\dagger b_j + \text{H.c.}) + J_z \sum_{\langle i,j\rangle} S_i^z S_j^z - J_{XY} \sum_{\langle i,j\rangle} \left(S_i^x S_j^x + S_i^y S_j^y\right), \tag{2.1}$$

where $a_i^\dagger$ and $b_i^\dagger$ are boson creation operators [15] at site i, the pseudospin operator is given as $\vec{S}_i = \frac{1}{2} B_i^\dagger \vec{\sigma} B_i$ with $B_i = (a_i, b_i)^t$ and the Pauli spin matrices $\vec{\sigma}$, and $\langle i,j\rangle$ stands for nearest-neighbor (NN) sites on the lattice. We consider a two-dimensional (2D) square lattice in this study. The first, t term in Hamiltonian (2.1) is the hopping term of the a and b atoms, the second, J_z term represents the interaction between atoms at the NN sites, and the third, J_{XY} term enhances the coherence

*ikuo@nitech.ac.jp

of the relative phases of the a and b atomic fields. From the definition of the Pauli matrix σ_z, it is obvious that the J_z term corresponds to a repulsive intraspecies interaction and an attractive interspecies interaction for $J_z > 0$.

The physical Hilbert space of the B-t-J model consists of states in which the total particle number at each site is strictly restricted to be less than unity. In order to incorporate this local constraint faithfully, we use the slave-particle representation [9,10],

$$a_i = \phi_i^\dagger \varphi_{i1}, \quad b_i = \phi_i^\dagger \varphi_{i2}, \tag{2.2}$$

$$(\phi_i^\dagger \phi_i + \varphi_{i1}^\dagger \varphi_{i1} + \varphi_{i2}^\dagger \varphi_{i2} - 1)|\text{phys}\rangle = 0, \tag{2.3}$$

where ϕ_i is a boson operator that *annihilates the hole* at site i, whereas φ_{1i} and φ_{2i} are bosons that represent the pseudospin degrees of freedom. $|\text{phys}\rangle$ is the physical state of the slave-particle Hilbert space.

The previous numerical study of the B-t-J model [9,10,16] showed that there appear various phases, including an SF with Bose-Einstein condensation and a state with pseudospin long-range order. For most of the parameter regions, QMC simulations show that the density fluctuation of particles at each lattice site is stable even in spatially inhomogeneous states like a phase-separated state. From this observation, we expect that the following term effectively appears,

$$H_V = \frac{V_0}{4} \sum_i ((\varphi_{1i}^\dagger \varphi_{1i} - \rho_{1i})^2 + (\varphi_{2i}^\dagger \varphi_{2i} - \rho_{2i})^2 + (\phi_i^\dagger \phi_i - \rho_{3i})^2), \tag{2.4}$$

where ρ_{1i}, etc., are the parameters that control the densities of a and b atoms at site i, and V_0 (>0) controls their fluctuations around the mean values. It should be remarked here that the expectation values of the particle numbers in the physical state $|\text{phys}\rangle$ are $\langle a_i^\dagger a_i\rangle \equiv \text{Tr}_{\text{phys}}(a_i^\dagger a_i) = \text{Tr}_{\text{phys}}(\varphi_{1i}^\dagger \varphi_{1i})$ and, similarly, $\langle b_i^\dagger b_i\rangle = \text{Tr}_{\text{phys}}(\varphi_{2i}^\dagger \varphi_{2i})$, where Tr_{phys} denotes the trace over states satisfying the local constraint, (2.3). Therefore constraint (2.3) requires that $\sum_{\sigma=1}^3 \rho_{\sigma i} = 1$ at each site i. The values of V_0 and $\rho_{\sigma i} (\sigma = 1,2,3)$ are to be determined, in principle, by t, J_z, J_{XY}, and the filling factor, but here we add H_V to H_{tJ} by hand and regard the parameter V_0 in H_V as a free parameter, whereas $\rho_{\sigma i} (\sigma = 1,2,3)$ are to be determined accurately by H_{tJ}. In other words, we take the extended B-t-J model $H_{tJ} + H_V$ as a canonical model and regard H_V as a residual one-site repulsion that cannot be incorporated by the hard-core constraint. However, we expect that the original B-t-J model has a phase diagram similar to that of the extended B-t-J model. See later remarks on this point.

By means of the path-integral method, the partition function Z is expressed as follows by introducing the imaginary time τ,

$$Z = \int [D\phi D\varphi_1 D\varphi_2] \exp\left[-\int d\tau (\bar\varphi_{1i}(\tau)\partial_\tau \varphi_{1i}(\tau) + \bar\varphi_{2i}(\tau)\partial_\tau \varphi_{2i}(\tau) + \bar\phi_i(\tau)\partial_\tau \phi_i(\tau) + H_{tJ} + H_V) \right], \tag{2.5}$$

where H_{tJ} and H_V are expressed by slave particles, (2.2), and the above path integral is evaluated under constraint (2.3). The direct QMC is not applicable to system (2.5) due to the Berry phases $(\bar\varphi \partial_\tau \varphi)$, etc., and therefore we separate the path-integral variables φ and ϕ as

$$\begin{aligned} \varphi_{1i} &= \sqrt{\rho_{1i} + \ell_{1i}} \exp(i\omega_{1i}), \\ \varphi_{2i} &= \sqrt{\rho_{2i} + \ell_{2i}} \exp(i\omega_{2i}), \\ \phi_i &= \sqrt{\rho_{3i} + \ell_{3i}} \exp(i\omega_{3i}) \end{aligned} \tag{2.6}$$

and then integrate out the (fluctuation of the) radial degrees of freedom, $\ell_{\sigma i}$ ($\sigma = 1,2,3$). By the existence of the term H_V, the integration can be performed straightforwardly. There exists a constraint like $\ell_{1i} + \ell_{2i} + \ell_{3i} = 0$ on performing the path integral over the radial degrees of freedom. But this constraint can be readily incorporated using a Lagrange multiplier, $\lambda_i(\tau)$,

$$\prod_\tau \delta(\ell_{1i} + \ell_{2i} + \ell_{3i}) = \int d\lambda_i e^{i\int d\tau (\ell_{1i}+\ell_{2i}+\ell_{3i})\lambda_i}.$$

The variables $\ell_{\sigma i}$ ($\sigma = 1,2,3$) also appear in H_{tJ}, but we ignore them by simply replacing $\varphi_{\sigma i} \to \sqrt{\rho_{\sigma i}} \exp(i\omega_{\sigma i})$, and then we have

$$\begin{aligned} &\int d\lambda_i d\ell_i e^{\int d\tau \sum_{\sigma=1}^3 (-V_0(\ell_{\sigma,i})^2 + i\ell_{\sigma,i}(\partial_\tau \omega_{\sigma,i} + \lambda_i))} \\ &= \int d\lambda_i e^{-\frac{1}{4V_0}\int d\tau \sum_\sigma (\partial_\tau \omega_{\sigma,i} + \lambda_i)^2}, \end{aligned} \tag{2.7}$$

where we have ignored terms like $\int d\tau \partial_\tau \omega_{\sigma,i}$ by the periodic boundary condition for the imaginary time. The resultant quantity on the right-hand side of (2.7) is positive definite, and therefore a numerical study by QMC can be performed without any difficulty. It should be remarked that the Lagrange multiplier λ_i in Eq. (2.7) behaves as a gauge field, i.e., the right-hand side of (2.7) is invariant under the "gauge transformation" $\omega_{\sigma,i} \to \omega_{\sigma,i} + \alpha_i$, $\lambda_i \to \lambda_i - \partial_\tau \alpha_i$. In the practical calculation, we show that all physical quantities are invariant under the above gauge transformation.

Here, remarks are in order.

(1) The direct QMC of system Z in Eq. (2.5) is impossible, as the Berry phases $\bar\varphi \partial_\tau \varphi$ are pure imaginary. However, by integrating over the density fluctuations $\ell_{\sigma i}$, the action becomes positive definite as Eq. (2.7) shows, and thus the QMC can be applied without any difficulty.

(2) In order to integrate over $\ell_{\sigma i}$, we have introduced the density-fluctuation term H_V. Terms effectively similar to H_V are generated from the terms in the Hamiltonian of the original B-t-J model, (2.1). For example, a rough estimation of the density fluctuation of the a atom $\delta\rho_{ai}$ gives

$$\left(t\frac{\mathcal{P}}{\rho_{ai}} + J_{XY}\sqrt{\rho_{ai}}\frac{\mathcal{Q}}{(\sqrt{\rho_{bi}})^3} \right)(\delta\rho_{ai})^2, \tag{2.8}$$

where ρ_{ai} (ρ_{bi}) is the mean value of the a-atom (b-atom) density, and the positive parameters $\mathcal{P}$ and $\mathcal{Q}$ are determined by the NN correlations of the phase degrees of freedom of the atomic fields like $\mathcal{P} = \langle \cos(\theta_{ai} - \theta_{aj})\rangle$, where θ_{ai} is the phase of the a-atom field. In the QMC in Sec. IV, we fix the values of t and J_{XY}, and the values of ρ_{ai} and ρ_{bi} are determined by the B-t-J model, (2.1), quite accurately. It

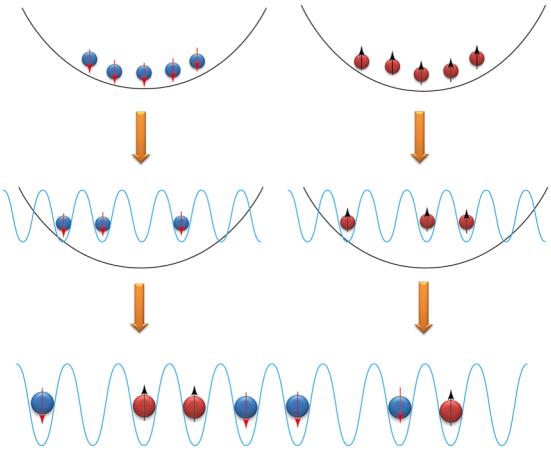

FIG. 1. (Color online) Experimental setup for two-component dipolar bosons in an OL. Dipole-dipole interactions generate long-range repulsive and attractive interactions between the two kinds of bosons.

is difficult to obtain the coefficient in Eq. (2.8) accurately, but it is expected that the coefficient in Eq. (2.8) is fairly stable against the variations of ρ_{ai} and ρ_{bi}, as we require the constraint $\rho_{ai} + \rho_{bi} = 1-$(constant hole density) in the calculation and also by the behavior of the correlators $\mathcal{P}$ and $\mathcal{Q}$. Furthermore, for the system $H_{tJ} + H_V$, we have verified by practical calculation that a change in the value of V_0 in H_V does not substantially influence the global phase diagram of the system, although the SF region increases slightly for smaller V_0 as greater density fluctuation stabilizes the phase degrees of freedom by the density-phase uncertainty principle. See Ref. [13], in particular, the left panels in Fig. 1 there. Thus it is naturally expected that the phase diagram of the constant-V_0 system obtained with the QMC faithfully describes the phase structure of the original B-t-J model as well as the extended B-t-J model with the H_V term.

(3) The partition function obtained by performing the integral in Eq. (2.7) depends on the local density of the bosons $\rho_{\sigma i}$. We treat the density difference $\Delta\rho_i \equiv \rho_{1i} - \rho_{2i} = \rho_{ai} - \rho_{bi}$ as a variational parameter *while keeping the one-site hole density fixed*; i.e., $\rho_{1i} + \rho_{2i} = \rho_{ai} + \rho_{bi} =$ constant. This treatment obviously precludes the possibility of a phase-separated state. The previous study, by means of a Gross-Pitaevskii equation and QMC [17], showed that such a phase-separated state does not appear in the B-t-J model, (2.1). Therefore this treatment is justified.

(4) The last remark concerns Hamiltonian (2.1) itself. Originally, the B-t-J model was derived as an effective model of the Bose-Hubbard model in the large on-site-repulsion limit. By integrating out the multiple-particle states at each site, the NN terms of the pseudospin interactions appear. At present, however, the interactions between atoms located at NN sites can be generated and their strength is controlled by using the DDIs. Thus Hamiltonian (2.1) can be regarded as the original Hamiltonian, and it is quite natural to add the Hubbard term H_V in Eq. (2.4) to H_{tJ}. In this case, the a and b atoms are not hard-core boson and their density can take arbitrary values. The effective model of the system is derived by a method similar to the one above, but use of the slave-particle representation is not needed.

As explained in Sec. I, we study Bose gases with DDIs in this paper. In Sec. II B, we briefly explain the DDI, which gives a long-range interaction between the z components of the pseudospin S^z.

B. Realization of long-range spin interactions via the DDI

When the atoms have a magnetic or electric dipole, terms describing the DDI [12] should be added to the B-t-J model Hamiltonian. We first consider a specific case in which the a atom has the upward dipole, whereas the b atom has the downward one, perpendicular to the OL. See Fig. 1. We regard this system as a canonical system and clarify its phase diagram in the subsequent sections. The system of a strongly correlated dipolar gas, which was recently realized in experiments, is considered in Sec. VI, because it has rather strong anisotropy in couplings.

The DDI is generally given as

$$\hat{H}_d = d^2 \frac{\hat{\mathbf{S}}_1 \cdot \hat{\mathbf{S}}_2 - 3(\hat{\mathbf{S}}_1 \cdot \hat{\mathbf{r}})(\hat{\mathbf{S}}_2 \cdot \hat{\mathbf{r}})}{4\pi r^3}, \tag{2.9}$$

where $d^2 = \mu_0(g\mu_B)^2$ (μ_0 being the magnetic permeability of the vacuum, g the Lande factor, and μ_B the Bohr magneton), $\hat{\mathbf{S}}_j (j = 1,2)$ is the dipole-moment vector of the jth atom, and $\hat{\mathbf{r}} = \frac{\mathbf{r}}{r}$ with the relative position vector $\mathbf{r}$ of the atoms. In the present canonical system, $\hat{\mathbf{S}}_1 // \hat{\mathbf{S}}_2$ and $\hat{\mathbf{S}}_1, \hat{\mathbf{S}}_2 \perp \mathbf{r}$, and therefore only the first term on the right-hand side of Eq. (2.9) contributes. In Fig. 1, an experimental manipulation for realizing the canonical system is shown schematically. First, we prepare independently the a boson with an up-polarized state and the b boson with a down-polarized state in two magnetic traps. Second, an OL is created in each trap. Finally, we combine these two systems quasistatically and lower the temperature. As a result of the strong repulsions between atoms and the finite hopping amplitude, the total particle number at each site of the OL is less than unity. Furthermore, due to the angular-momentum conservation, the direction of the dipole does not change under the hopping of atoms.

Though the DDI has a long-range nature, we consider only the NN coupling and the next-nearest-neighbor (NNN) coupling in the OL. In the present dipole configuration, the DDI reduces the interspecies attraction and intraspecies repulsion. Thus $\hat{H}_d$ in Eq. (2.9) effectively generates the terms

$$\begin{aligned} V_{\mathrm{DDI}} &= \sum_{\langle i,j\rangle} V_{\mathrm{NN}}(n_{ai}n_{aj} + n_{bi}n_{bj} - n_{ai}n_{bj} - n_{bi}n_{aj}) \\ &\quad + \sum_{\langle\langle i,j\rangle\rangle} V_{\mathrm{NNN}}(n_{ai}n_{aj} + n_{bi}n_{bj} - n_{ai}n_{bj} - n_{bi}n_{aj}) \\ &= \sum_{\langle i,j\rangle} V_{\mathrm{NN}} S_i^z S_j^z + \sum_{\langle\langle i,j\rangle\rangle} V_{\mathrm{NNN}} S_i^z S_j^z, \end{aligned} \tag{2.10}$$

where $n_{ai} = a_i^\dagger a_i$, etc., we have used $S_i^z = \frac{1}{2}(n_{ai} - n_{bi})$, and $\langle\langle i,j\rangle\rangle$ stands for NNN sites. The parameters V_{NN} and V_{NNN} are given by the overlap integral of the lowest level Wannier functions (s wave) on the OL sites. The V_{DDI} term in Eq. (2.10)

is to be added to the Hamiltonian of the B-t-J model. In the following studies, we consider the system described by $H_{\mathcal{T}} \equiv H_{tJ} + V_{\rm DDI}$.

III. GUTZWILLER VARIATIONAL METHOD

Mean-field theory (MFT) is widely used to study phase diagrams of condensed matter systems. In this section, we employ the Gutzwiller variational method, which is a kind of MFT, to investigate the phase diagram of the system $H_{\mathcal{T}}$ at vanishing temperature (T). From the results of previous studies [7], we expect the appearance of two kinds of solid order, i.e., checkerboard solid (CBSo) and striped solid (SSo) order, in certain parameter regions. The solid order is the spatial pattern of the atomic densities and is nothing but the pseudospin order in the B-t-J model, as S_i^z is given by $S_i^z = \frac{1}{2}(n_{ai} - n_{bi})$.

As the present model describes the strong on-site repulsion limit, the physical state at each site consists of the following three states: $|a\rangle$ (single a boson), $|b\rangle$ (single b boson), and $|0\rangle$ (empty = hole). By using the above three basis vectors, we construct a variational wave function corresponding to the state with the double SF (2SF) and/or the CBSo,

$$
\begin{aligned}
&|\Phi_{\rm 2SF-CB}\rangle \\
&= \Pi_{i\in A}\left[\sin\frac{\theta_i}{2}\left(\sin\frac{\chi_i}{2}a_i^\dagger + \cos\frac{\chi_i}{2}b_i^\dagger\right) + \cos\frac{\theta_i}{2}\right]|0\rangle \\
&\quad\times \Pi_{i\in B}\left[\sin\frac{\theta_i}{2}\left(\cos\frac{\chi_i}{2}a_i^\dagger + \sin\frac{\chi_i}{2}b_i^\dagger\right) + \cos\frac{\theta_i}{2}\right]|0\rangle,
\end{aligned}
\tag{3.1}
$$

where the label A (B) stands for the even (odd) sublattice, and the parameters (θ_i, χ_i) are to be determined by the variational method. At the MFT level, we reduce the local variables θ_i and χ_i to global ones, (θ_A, θ_B) and (χ_A, χ_B). It should be noted that the state of the wave function, (3.1), has the discrete translational symmetries of double-lattice spacing in both the x and the y directions.

Another possible solid order is the SSo. The variational wave function that describes the SSo and 2SF is given as

$$
\begin{aligned}
&|\Phi_{\rm 2SF-SSo}\rangle \\
&= \Pi_{i\in x_o}\left[\sin\frac{\theta_i}{2}\left(\sin\frac{\chi_i}{2}a_i^\dagger + \cos\frac{\chi_i}{2}b_i^\dagger\right) + \cos\frac{\theta_i}{2}\right]|0\rangle \\
&\quad\times \Pi_{i\in x_e}\left[\sin\frac{\theta_i}{2}\left(\cos\frac{\chi_i}{2}a_i^\dagger + \sin\frac{\chi_i}{2}b_i^\dagger\right) + \cos\frac{\theta_i}{2}\right]|0\rangle,
\end{aligned}
\tag{3.2}
$$

where the site label x_o (x_e) denotes an odd (even) line sublattice in the x direction corresponding to the stripe pattern. The above wave function, (3.3), has the discrete translational symmetry of double-lattice spacing in the x direction and the ordinary one of single-lattice spacing in the y direction.

From the wave functions, (3.1) and (3.3), we calculate the expectation value of the Hamiltonian $H_\mu \equiv H_{\mathcal{T}} - \mu\sum(a_i^\dagger a_i + b_i^\dagger b_i)$, where μ is the chemical potential, and obtain

$$
\begin{aligned}
\frac{E_{\rm CS}}{J_{XY}N_s} &\equiv \langle\Phi_{\rm 2SF-CB}|H_\mu|\Phi_{\rm 2SF-CS}\rangle/(J_{XY}N_s) \\
&= -\tilde{t}\sin^2\theta\sin\chi + 2(-\tilde{J}_{z\rm NN} + \tilde{J}_{z\rm NNN})\sin^4\frac{\theta}{2}\cos^2\chi \\
&\quad - \frac{1}{8}\sin^4\theta\sin^2\chi - \mu\sin^2\frac{\theta}{2},
\end{aligned}
\tag{3.3}
$$

$$
\begin{aligned}
\frac{E_{\rm SS}}{J_{XY}N_s} &\equiv \langle\Phi_{\rm 2SF-SSo}|H_\mu|\Phi_{\rm 2SF-SSo}\rangle/(J_{XY}N_s) \\
&= -\frac{1}{2}\tilde{t}\sin^2\theta(1+\sin\chi) - 2\tilde{J}_{z\rm NNN}\sin^4\frac{\theta}{2}\cos^2\chi \\
&\quad - \frac{1}{8}\sin^4\theta\sin^2\chi - \mu\sin^2\frac{\theta}{2}.
\end{aligned}
\tag{3.4}
$$

In Eqs. (3.3) and (3.4), the variational energies are normalized by $J_{XY}N_s$, where N_s is the total number of sites, and thus, $\tilde{t} \equiv t/J_{XY}$, $\tilde{J}_{z\rm NN} \equiv J_{z\rm NN}/J_{XY}$, and $\tilde{J}_{z\rm NNN} \equiv J_{z\rm NNN}/J_{XY}$, where $J_{z\rm NN} \equiv J_z + V_{\rm NN}$ and $J_{z\rm NNN} \equiv V_{\rm NNN}$.

From Eqs. (3.3) and (3.4), it is rather straightforward to obtain the lowest energy states by varying the values of θ and χ, and then the global phase diagram is obtained. The obtained phase diagram is shown in the top panel in Fig. 2, where $v_2 = J_{z\rm NNN}/J_{z\rm NN}$. The bottom panel in Fig. 2 is the phase diagram in the (μ-$\tilde{J}_{z\rm NN}$) plane. It is obvious that at the MFT level, the SS does not form and the solid phases, the CBSo and SSo, exist only at the vanishing hole density. On the other hand, the 2SF phase has a finite hole density; in particular, the minimal density is 30%. The above results are in agreement with the previous MFT results for the one and two-component Bose-Hubbard models in Refs. [6] and [11], which showed that the SS does not form and a direct phase transition from the CBSo to SSo takes place.

IV. QUANTUM MONTE CARLO SIMULATION

In this section, we study the extended B-t-J model, $H_{\mathcal{T}} + H_V$, by QMC. In particular, we are interested in the global phase diagram and the region in which the SS forms. As explained in Sec. I, we expect that SSs with different solid orders appear as a result of DDIs.

For the practical QMC, we put the lattice spacing of the OL, a_L, to the unit of length. We also introduce a discretized lattice for the imaginary-time τ with the lattice spacing $\Delta\tau$. Thus, the model is defined on a three-dimensional (3D) space-time lattice, and hereafter we denote the site of the 3D lattice i, j, etc.

The previous study [17] on the B-t-J model H_{tJ} shows that holes are distributed quite homogeneously except for a very specific parameter region in which a phase-separated state forms. Therefore, we assume a homogeneous distribution of holes also in the present system and put the hole density at each site to 30%, i.e., $\rho_{3,i} = \rho_3 = 0.3$. On the other hand, the density difference of the a and b atoms at site i, $\Delta\rho_i = \rho_{1i} - \rho_{2i}$, is a variational variable and is determined by the maximal free-energy condition. See later discussion.

The effective lattice model of the extended B-t-J model $H_{\mathcal{T}} + H_V$ is derived from Eqs. (2.5) and (2.7). The partition

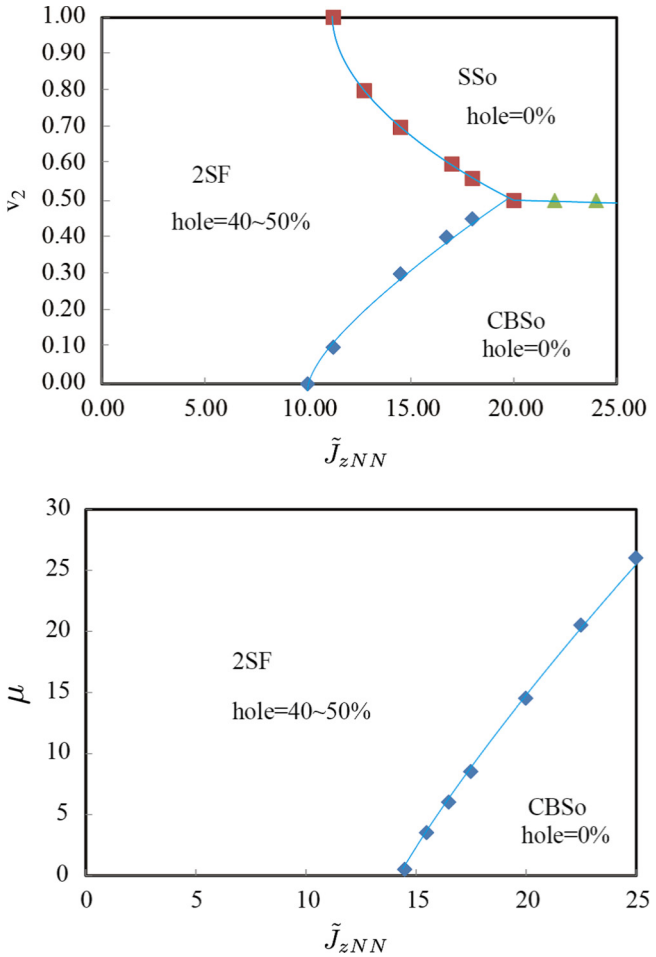

FIG. 2. (Color online) Phase diagrams at $T = 0$ in the grand-canonical ensemble obtained by the MFT. $\mu = 0$ phase diagram in the $(\tilde{J}_{zNN} - v_2)$ plane (top) and in the $(\mu\text{-}\tilde{J}_{zNN})$ plane for $v_2 \equiv J_{zNNN}/J_{zNN} = 0.3$. In the MFT phase diagrams, the SS does not exist.

function and action of the effective model are given as [13,17]

$$Z_{qXY} \equiv \int \Pi_{\alpha=1,2,3}[d\omega_{\alpha,i}][d\lambda_i]e^{A_{qXY}},$$
$$A_{qXY} = A_\tau + A_L(e^{i\Omega_\sigma}, e^{-i\Omega_\sigma}) + A_{zNN}, \tag{4.1}$$

where

$$A_\tau = -c_\tau \sum_i \sum_{\sigma=1}^{3} \cos(\omega_{\sigma,i+\hat{\tau}} - \omega_{\sigma,i} + \lambda_i), \tag{4.2}$$

$$A_L = \sum_{\langle i,j\rangle} (C_1 \cos(\Omega_{1,i} - \Omega_{1,j}) + C_2 \cos(\Omega_{2,i} - \Omega_{2,j}) + C_3 \cos(\Omega_{3,i} - \Omega_{3,j})), \tag{4.3}$$

and

$$A_{zNN} = -J_{zNN}\Delta\tau \sum_{\langle i,j\rangle} \Delta\rho_i \Delta\rho_j - J_{zNNN}\Delta\tau \sum_{\langle\langle i,l\rangle\rangle} \Delta\rho_i \Delta\rho_l, \tag{4.4}$$

where $\langle\cdots\rangle$ stands for NN sites in the 2D spatial lattice, and $\langle\langle\cdots\rangle\rangle$, NNN sites. The dynamical variables $\Omega_{\alpha,i}$ $(\alpha = 1,2,3)$ are related to the phases $\omega_{\alpha,i}$ as

$$\Omega_{1,i} = \omega_{1,i} - \omega_{2,i},$$
$$\Omega_{2,i} = \omega_{1,i} - \omega_{3,i},$$
$$\Omega_{3,i} = \omega_{2,i} - \omega_{3,i}.$$

As explained in Sec. II, the partition function in Eq. (4.1) has been derived by integrating out the amplitude modes of slave-particle fields. As a result, the coefficients in the action A_{qXY} depend on the local variational parameter $\{\Delta\rho_i\}$ and they are explicitly given as

$$c_\tau = \frac{1}{V_0\Delta\tau},$$
$$C_1 = J_{XY}\rho_3\Delta\tau\sqrt{((1-\rho_3)^2 - (\Delta\rho_i)^2)((1-\rho_3)^2 - (\Delta\rho_j)^2)},$$
$$C_2 = t\rho_3\Delta\tau\sqrt{(1-\rho_3+\Delta\rho_i)(1-\rho_3+\Delta\rho_j)},$$
$$C_3 = t\rho_3\Delta\tau\sqrt{(1-\rho_3-\Delta\rho_i)(1-\rho_3-\Delta\rho_j)}.$$

By the relation $1/(k_BT) = L\Delta\tau$, where L is the linear system size, $\Delta\tau$ has dimension 1/(energy) and the low-temperature limit is realized for $L \to \infty$. We put $c_\tau = 2$ in the practical calculation, and thus $k_BT = (c_\tau V_0)/L = 2V_0/L$. Here it should be noted that a change in the value of V_0 results in a change in c_τ. A previous study [13] showed that the global phase structure of the system H_{tJ} is stable against change in the value of c_τ with fixed $\Delta\tau$. In general, for a smaller value of V_0, i.e., a larger c_τ, the parameter region of the SF is enlarged [13].

The partition function Z_{qXY} in Eq. (4.1) is a functional of $\Delta\rho_i$; i.e., $Z_{qXY} = Z_{qXY}(\{\Delta\rho_i\})$. We expect that $\Delta\rho_i$ behave as variational variables and determine them under the optimal free-energy condition. In the practical calculation, we performed the local update of $\Delta\rho_i$ by QMC simulation and obtained

$$[Z_{qXY}] \equiv \int [d\Delta\rho_i] Z_{qXY}(\{\Delta\rho_i\}). \tag{4.5}$$

However, in the updates of the QMC, $\{\Delta\rho_i\}$ are quite stable [17] for given values of parameters in the action A_{qXY}. This fact indicates that $\{\Delta\rho_i\}$ should be regarded as variational parameters rather than dynamical variables. For the QMC, we employed the ground-canonical ensemble, and therefore the numbers of a and b bosons, N_a and N_b, are not conserved independently in QMC updates, although the total atomic number $N_a + N_b$ is conserved.

In the practical calculation, we employed the standard Metropolis algorithm with the local update [18]. The typical sweep for the measurement is (50 000–100 000) × (10 samples), and the acceptance ratio is 40–50%. Errors are estimated from 10 samples by the jackknife method.

To obtain the phase diagram, we calculated the internal energy E and specific heat C, which are defined as

$$E = \langle (A_L + A_{zNN})\rangle/L^3,$$
$$C = \langle ((A_L + A_{zNN}) - L^3E)^2\rangle/L^3. \tag{4.6}$$

To identify various phases, we also calculated the following pseudospin correlation function, boson correlation function,

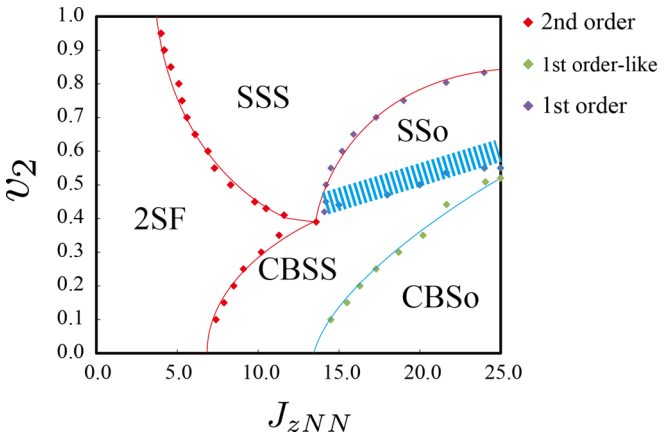

FIG. 3. (Color online) Phase diagram at $T = 0$ obtained with the QMC, which includes the effects of quantum fluctuations. We consider the case with a homogeneous hole density $\rho_3 = 0.3$, $c_\tau = 2.0$, $C_1 = 2$, and $t = 20$. We introduce the amplitude ratio, $v_2 = J_{z\mathrm{NNN}}/J_{z\mathrm{NN}}$. There exist five phases including two SS phases, i.e., the CBSS and SSS. In the hatched (blue) region, coexistence of the CBSS and SSo is verified. Hereafter, for the unit of energy, we put $2V_0 = 1$, i.e., $\Delta\tau = 1$.

and, also, density-difference correlation function,

$$
\begin{aligned}
G_S(r) &= \frac{1}{L^3}\sum_{i_0}\langle e^{i\Omega_{1,i_0}} e^{-i\Omega_{1,i_0+r}}\rangle,\\
G_a(r) &= \frac{1}{L^3}\sum_{i_0}\langle e^{i\Omega_{2,i_0}} e^{-i\Omega_{2,i_0+r}}\rangle,\\
G_b(r) &= \frac{1}{L^3}\sum_{i_0}\langle e^{i\Omega_{3,i_0}} e^{-i\Omega_{3,i_0+r}}\rangle,\\
G_{\mathrm{dd}}(r) &= \frac{1}{L^3}\sum_{i_0}\langle \Delta\rho_{i_0}\Delta\rho_{i_0+r}\rangle,
\end{aligned}
\tag{4.7}
$$

where sites i_0 and $i_0 + r$ are located in the same spatial 2D lattice. The order of the phase transition was identified by calculating the density of state $N(E)$, which is defined by

$$
[Z_{\mathrm{qXYZ}}] = \int dE N(E) e^{-E}. \tag{4.8}
$$

If $N(E)$ has a single peak at the transition point, the phase transition is of second order. On the other hand, a double-peak shape of $N(E)$ indicates the existence of a first-order phase transition.

In Fig. 3, we show the global phase diagram obtained by the QMC for $c_\tau = 2.0$, $C_1 = 2$, and $t = 20$. By calculating the density of states $N(E)$, the order of the phase transitions has been determined as indicated in Fig. 3. Typical behaviors of the specific heat C and the internal energy E are shown in Fig. 4 in the $(v_2 - J_{z\mathrm{NN}})$ plane, where $v_2 = J_{z\mathrm{NNN}}/J_{z\mathrm{NN}}$. The density of states, $N(E)$, on typical critical points is shown in Fig. 5. Furthermore, some correlation functions and density-difference $\{\Delta\rho_i\}$ snapshots, which were used for the identification of each phase, are exhibited in Fig. 6.

As the phase diagram in Fig. 3 shows, there exist five phases: 2SF, checkerboard supersolid (CBSS), striped supersolid (SSS), CBSo, and SSo. In particular, the two kinds of SSs form in the intermediate parameter regime between the genuine SF and the solids. The correlation functions indicating the existence of SSs are shown in Fig. 6.

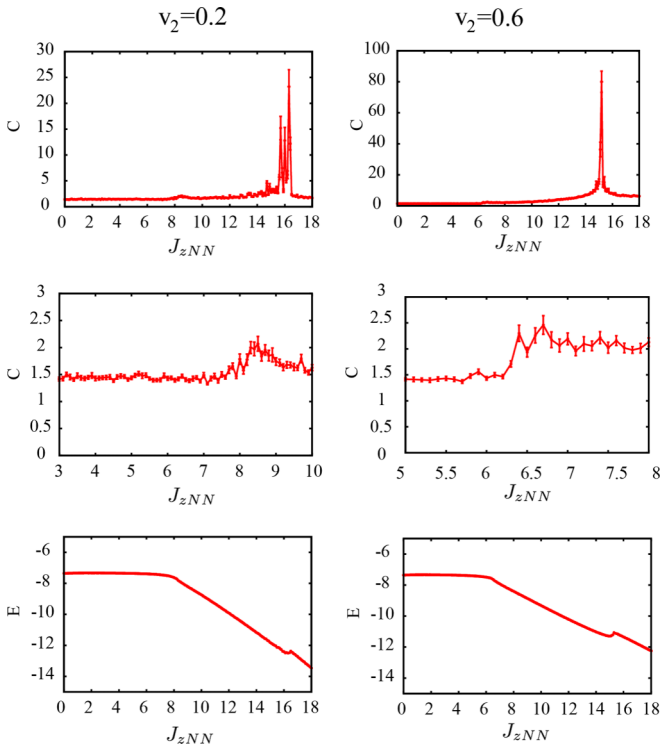

FIG. 4. (Color online) Specific heat C and internal energy E for $v_2 = 0.2$ and 0.6. For both cases, there exist two phase transitions. See the phase diagram in Fig. 3. System size $L = 16$.

In contrast to the MFT phase diagram in Fig. 2, the SSs form in a rather large parameter region of the phase diagram in Fig. 3. This means that quantum fluctuations play an

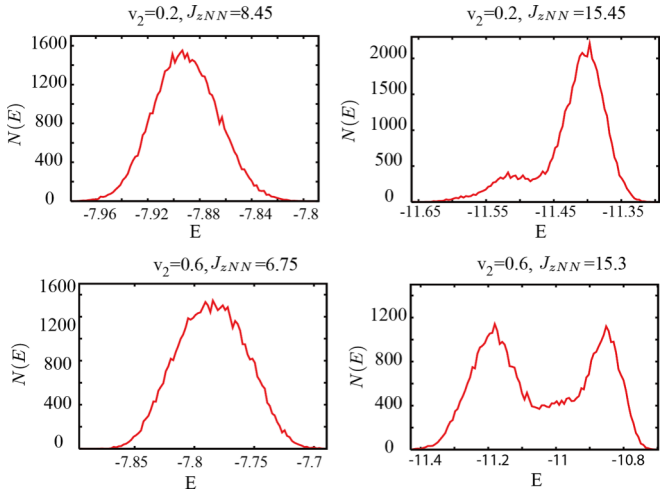

FIG. 5. (Color online) Density of state $N(E)$ used to determine the order of the phase transitions. A single peak of $N(E)$ at the phase transition point indicates a second-order phase transition; a double-peak, a first-order phase transition. $v_2 = J_{z\mathrm{NNN}}/J_{z\mathrm{NN}}$, and system size $L = 16$.

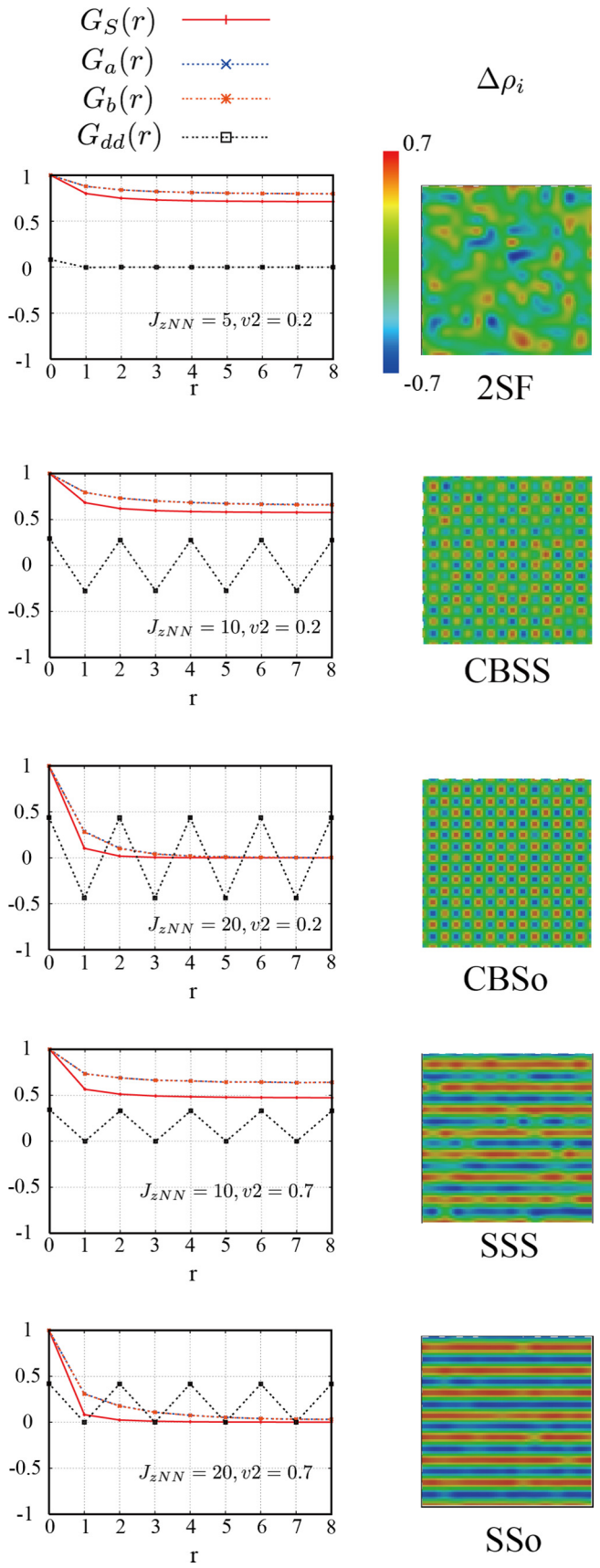

FIG. 6. (Color online) Various correlation functions and snapshots used to identify physical properties of each phase. Density difference $\Delta\rho_i \equiv n_{a,i} - n_{b,i}$.

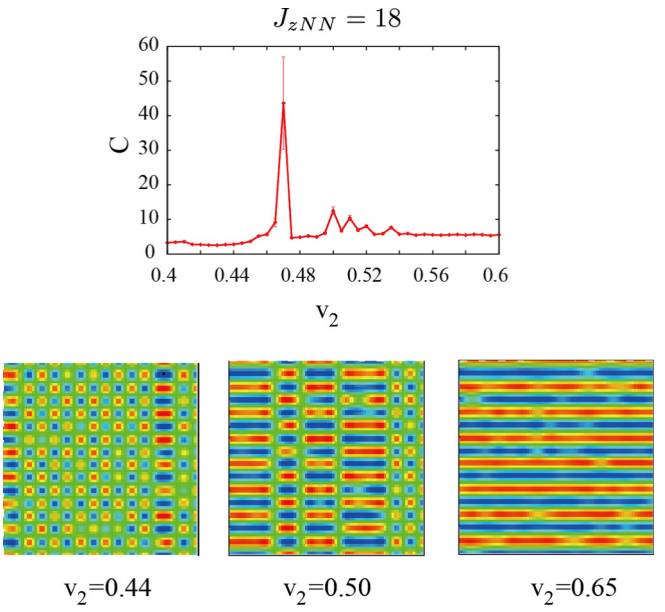

FIG. 7. (Color online) Specific heat as a function of v_2 for $J_{zNN} = 18$. Besides the large peak at $v_2 \simeq 0.47$, which indicates the existence of a first-order phase transition, there are several small peaks from $v_2 = 0.48$ to $v_2 = 0.54$. The snapshot for $v_2 = 0.50$ indicates a phase of CBSS and SSo coexistence.

essentially important role for the coexistence of the SF and solid order. In other words, in SS states, both the density of particles and the SF order parameter (i.e., the phase of the boson fields) fluctuate as required by the quantum uncertainty principle, but their fluctuations are rather moderate and thus both orders are preserved intact. It is interesting to note that the parameter region of the SSS is larger than that of the CBSS. This means that the 1D structure of the stripe is more compatible with the SF rather than the CB as is physically expected.

As far as the phase diagram in Fig. 3 shows, there is no direct phase transition from the CBSo and SSo. In Ref. [19], a similar phase diagram was reported for the single-component Bose-Hubbard model. There the CBSo and SSo are separated by a simple SF phase. In the present system, however, the CBSS exists between the CBSo and the SSo.

By practical calculation, we have found that an interesting "phase" exists between the CBSS and the SSo, which is indicated by the hatched (blue) region in the phase diagram in Fig. 3. The specific heat C for $J_{zNN} = 18$ has the behavior shown in Fig. 7. It is obvious that there exists a first-order phase transition at $v_2 = \frac{J_{zNN}}{J_{zNNN}} \simeq 0.47$, and the CBSo terminates there. As the value of v_2 is increased from 0.47, several small peaks appear in C till $v_2 \simeq 0.54$. Snapshots are quite useful to understand what happens in this region. See Fig. 7; in particular, the snapshot of $v_2 = 0.50$. Small regions of the CBSo and SSo coexist there in a phase-separated form, and we verified that the spatial pattern of these small regions is rather stable under the MC updates. Our observation indicates that there exist several (meta)stable "mixed crystals" of the CBSo and SSo between the CBSS and the SSo, and this mixing of the solid order destroys the SF. For the 2D J_1-J_2

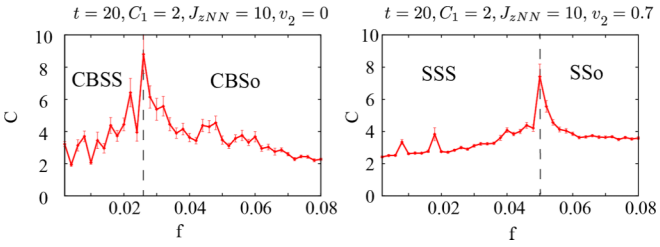

FIG. 8. (Color online) Specific heat as a function of the magnetic flux f. As f is increased, SF is lost. However, the solid orders are stable against the magnetic field.

Heisenberg model, it was expected that a quantum spin liquid exists between the Néel state and the stripe antiferromagnetic state [20]. The DDI in Eq. (2.10) has a similar structure to the above J_1-J_2 Heisenberg model, but we think the present mixed crystals are different from the quantum liquid, as the spatial pattern is stable. This is a result of the Ising-type spin coupling of $V_{\rm DDI}$, in contrast to the O(3) symmetric one in the J_1-J_2 Heisenberg model.

Nowadays, it is possible to apply an artificial external magnetic field to an atomic system in an OL by rotating the system or using lasers [21]. Atomic systems in an artificial magnetic field mimic superconducting systems, systems of the quantum Hall effect, etc., and therefore they are one of the most interesting subjects in cold-atomic physics. In this section, we study the (in)stability of SSs in an external magnetic field. We expect that the stability depends on the type of solid order of the SSs.

In the practical calculation, we used the symmetric gauge for the vector potential. The magnetic flux per plaquette of the OL is denoted $2\pi f$. In Fig. 8, we show the specific heat as a function of the strength of the magnetic field f. For the CBSS, the SF is lost at $f \simeq 0.025$, and for the SSS $f \simeq 0.055$. This result means that the SSS is more robust than the CBSS as expected from the phase diagram in Fig. 3.

V. MC SIMULATION OF A t-J-LIKE MODEL REALIZED BY COLD ATOMS IN AN OPTICAL LATTICE

In this section we focus on the experiment by de Paz *et al.* [2]. They succeeded in creating NNN pseudospin interactions by using the DDI of ^{52}Cr with total spin $s = 3$. In the experiment, doubly occupied states were excluded by the strong on-site repulsion. Furthermore, by applying an external magnetic field, the two states with spin component $m_s = -3$ and $m_s = -2$ in the direction of the magnetic field dominate the system. Thus the reduced DDI is regarded as a pseudospin interaction similar to that in the t-J model. The resultant atomic system of ^{52}Cr is a strongly correlated system and is well described by the B-t-J model.

However, as shown by the calculation in Ref. [2], the resultant B-t-J model has anisotropy in both the hopping amplitudes and the pseudospin interactions. Thus we call this the *t-J-like model* hereafter. We carried out a detailed study of the t-J-like model by QMC and obtained the phase structure of the t-J-like model in the parameter regime realized in the experiment.

The effective action, Eq. (4.1), changes to the following one by the anisotropy,

$$\begin{aligned} A_{t\text{-}J\text{-like}} = &-\sum_{\tau,i} c_\tau \cos(\theta_{a,i} - \theta_{a,i+\tau}) + c_\tau \cos(\theta_{b,i} - \theta_{b,i+\tau}) \\ &+ \sum_{i,j\in \mathrm{NNN}} C_{xy,j} \cos\left((\theta_{a,i} - \theta_{b,i}) - (\theta_{a,j} - \theta_{b,j})\right) \\ &- \sum_{i,j\in \mathrm{NN}} C_{2,j}\left(\cos(\theta_{a,i} - \theta_{a,j}) + \cos(\theta_{b,i} - \theta_{b,j})\right) \\ &+ \sum_{i,j\in \mathrm{NNN}} C_{z,j}\Delta\rho_i \Delta\rho_j, \end{aligned} \tag{5.1}$$

where

$$\begin{aligned} C_{xy,j} &= -\tfrac{1}{2} V_{ij} \tfrac{1}{4} \Delta\tau \sqrt{\left(\rho_0^2 - \Delta\rho_i^2\right)\left(\rho_0^2 - \Delta\rho_j^2\right)}, \\ C_{2,j} &= t_j \tfrac{1}{2} \Delta\tau \sqrt{(\rho_0 - \Delta\rho_i)(\rho_0 - \Delta\rho_j)}, \\ C_{z,j} &= V_{ij}\Delta\tau, \end{aligned} \tag{5.2}$$

and the anisotropic couplings t_j and $V_{i,j}$ are given as

$$V_{i,j} = \begin{cases} 0.8W_0 & (j = i + \hat{x}, i - \hat{x}), \\ -1.8W_0 & (j = i + \hat{y}, i - \hat{y}), \\ -0.11W_0 & (j \in \mathrm{NNN}), \end{cases} \tag{5.3}$$

$$t_j = \begin{cases} 3.66t & (j = i + \hat{x}, i - \hat{x}), \\ t & (j = i + \hat{y}, i - \hat{y}), \end{cases} \tag{5.4}$$

with

$$W_0 = \frac{\mu_0 \mu_B^2}{\pi (a_L/2)^3}, \tag{5.5}$$

where μ_B is the Bohr magneton and μ_0 is the magnetic permeability of the vacuum as before. The proposed t-J-like model in Ref. [2] has an additional effective Zeeman coupling along S^z, but we ignore it in the present study because we are interested in the genuine effect of the DDI.

For the practical calculation, we regard W_0 as a free parameter and put the hole density $\rho_0 = 0.3$. The strength of the dipole-induced pseudospin interaction relative to the hopping amplitude t determines the equilibrium state.

In the experiment, it was observed that there exists a density difference between the $m_s = -3$ and the $m_s = -2$ states at equilibrium, and this phenomenon was considered to be a result of the DDI.

In Fig. 9, we show the behaviors of the specific heat C for the t-J-like model with the energy unit $t = 2$. The obtained specific heat exhibits the existence of a second-order phase transition at $W_{0c} \simeq 1.1$. We also calculated the density-difference correlation function $G_{\rm dd}(r)$ defined by Eq. (4.7). From the density-difference correlation function shown in Fig. 9, it is obvious that $G_{\rm dd}(r) \to$ finite (0) as $r \to$ large for $W_0 > W_{0c}$ ($W_0 < W_{0c}$); i.e., the density of one atom is globally larger than that of the other for $W_0 > W_{0c}$, whereas an equal density distribution is realized for $W_0 < W_{0c}$. This is the direct result of the dipolar intersite spin interaction and is in agreement with the experimental observation. Density snapshots for $W_0 > W_{0c}$ and $W_0 < W_{0c}$ are shown in Fig. 9.

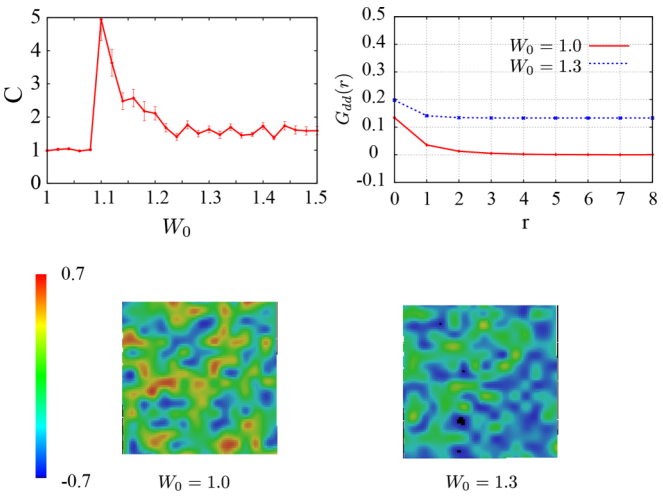

FIG. 9. (Color online) Top left: Specific heat with $t = 2$, $c_\tau = 2$. System size $L = 16$. Top right: Two typical behaviors of the density-difference correlation. Each of the two states is at equilibrium. Bottom left: Snapshot of the solid order (density difference) for $W_0 = 1.0$. Bottom right: Snapshot of the solid order for $W_0 = 1.3$. It seems that neither case has a clear solid order, but we verified that the density pattern is quite stable for the MC update.

No specific spatial pattern is observed, in contrast to the case studied in Sec. IV.

VI. CONCLUSION

In this paper, we have studied the extended B-t-J model of two-component bosons with the long-range DDI. We show that the DDI can generate additional pseudospin interactions by controlling the directions of the dipoles of the a and b atoms. We have studied the global phase diagram of the extended B-t-model by means of the Gutzwiller variational method and the QMC. The phase diagrams obtained indicate that quantum fluctuation is an essential ingredient for the realization of SSs. The QMC predicts two kinds of SS states, one of which is the CBSS and the other the SSS, and the latter stems from the long-range nature of the DDI. A detailed study of the phase boundary of the CBSS and SSo has also been reported.

Finally, we have investigated the t-J-like model, which is expected to describe the strongly correlated system recently realized in experiments [2]. By QMC, we confirmed the existence of a phase transition as the strength of the DDI is increased. In a state with the DDI stronger than the critical one, an imbalance of the density of atoms, which is nothing but a finite pseudospin order in the z direction, appears. The results obtained are consistent with the experimental findings.

ACKNOWLEDGMENT

This work was partially supported by a Grant-in-Aid for Scientific Research from the Japan Society for the Promotion of Science (No. 26400246).

[1] For review, see, e.g., I. Bloch, J. Dalibard, and W. Zwerger, Rev. Mod. Phys. **80**, 885 (2008); M. Lewenstein, A. Sanpera, V. Ahufinger, B. Damski, A. S. De, and U. Sen, Adv. Phy. **56**, 243 (2008).

[2] See, for example, A. de Paz, A. Sharma, A. Chotia, E. Maréchal, J. H. Huckans, P. Pedri, L. Santos, O. Gorceix, L. Vernac, and B. Laburthe-Tolra, Phys. Rev. Lett. **111**, 185305 (2013); B. Yan, S. A. Moses, B. Gadway, J. P. Covey, K. R. A. Hazzard, A. M. Rey, D. S. Jin, and J. Ye, Nature (London) **501**, 521 (2013).

[3] See, for example, E. Zohar and B. Reznik, Phys. Rev. Lett. **107**, 275301 (2011); K. Kasamatsu, I. Ichinose, and T. Matsui, *ibid.* **111**, 115303 (2013).

[4] See for example, O. Fialko, B. Opanchuk, A. I. Sidorov, P. D. Drummond, and J. Brand, arXiv:1408.1163v2, and references cited therein.

[5] A. F. Andreev and I. M. Lifshitz, Sov. Phys. JETP **29**, 1107 (1969).

[6] G. G. Batrouni, R. T. Scalettar, G. T. Zimanyi, and A. P. Kampf, Phys. Rev. Lett. **74**, 2527 (1995).

[7] K. Góral, L. Santos, and M. Lewenstein, Phys. Rev. Lett. **88**, 170406 (2002); V. W. Scarola and S. Das Sarma, *ibid.* **95**, 033003 (2005); C. Menotti, C. Trefzger, and M. Lewenstein, *ibid.* **98**, 235301 (2007); K.-K. Ng and Y.-C. Chen, Phys. Rev. B. **77**, 052506 (2008); I. Danshita and C. A. R. Sa de Melo, Phys. Rev. Lett. **103**, 225301 (2009); B. Capogrosso-Sansone, C. Trefzger, M. Lewenstein, P. Zoller, and G. Pupillo, *ibid.* **104**, 125301 (2010); K.-K. Ng, Phys. Rev. B. **82**, 184505 (2010); H. Ozawa and I. Ichinose, Phys. Rev. A. **86**, 015601 (2012).

[8] M. Boninsegni, Phys. Rev. Lett. **87**, 087201 (2001); Phys. Rev. B **65**, 134403 (2002).

[9] Y. Nakano, T. Ishima, N. Kobayashi, K. Sakakibara, I. Ichinose, and T. Matsui, Phys. Rev. B **83**, 235116 (2011).

[10] Y. Nakano, T. Ishima, N. Kobayashi, T. Yamamoto, I. Ichinose, and T. Matsui, Phys. Rev. A **85**, 023617 (2012).

[11] E. Altman, W. Hofstetter, E. Demler, and M. D. Lukin, New J. Phys. **5**, 113 (2003).

[12] T. Lahaye, C. Menotti, L. Santos, M. Lewenstein, and T. Pfau, Rep. Prog. Phys. **72**, 126401 (2009).

[13] Y. Kuno, K. Kataoka, and I. Ichinose, Phys. Rev. B **87**, 014518 (2013).

[14] For the Mott-insulator region, see A. B. Kuklov and B. V. Svistunov, Phys. Rev. Lett. **90**, 100401 (2003); L. M. Duan, E. Demler, and M. D. Lukin, *ibid.* **91**, 090402 (2003).

[15] It is rather straightforward to treat a_i and b_i as hard-core bosons as in Refs. [9] and [10]. As we impose the local constraint excluding the doubly occupied state in the following calculation, the results obtained are qualitatively the same.

[16] K. Kataoka, Y. Kuno, and I. Ichinose, J. Phys. Soc. Jpn. **81**, 124502 (2012).

[17] Y. Kuno, K. Suzuki, and I. Ichinose, J. Phys. Soc. Jpn. **83**, 074501 (2014).

[18] N. Metropolis, A. W. Rosenbluth, M. N. Rosenbluth, A. M. Teller, and E. Teller, J. Chem. Phys. **21**, 1087 (1953); J. M.

Thijssen, *Computational Physics* (Cambridge University Press, Cambridge, 1999).

[19] F. Hebert, G. G. Batrouni, R. T. Scalettar, G. Schmid, M. Troyer, and A. Dorneich, Phys. Rev. B. **65**, 014513 (2001).

[20] H.-C. Jiang, H. Yao, and L. Balents, Phys. Rev. B. **86**, 024424 (2012).

[21] D. Jaksch and P. Zoller, New J. Phys. **5**, 56 (2003); Y.-J. Lin, R. L. Compton, K. Jimnez-Garca, J. V. Porto, and I. B. Spielman, Nature **462**, 628 (2009); M. Aidelsburger, M. Atala, M. Lohse, J. T. Barreiro, B. Paredes, and I. Bloch, Phys. Rev. Lett. **111**, 185301 (2013); H. Miyake, G. A. Siviloglou, C. J. Kennedy, W. C. Burton, and W. Ketterle, *ibid.* **111**, 185302 (2013).